Model-based Spatial Harmonic Compensation in Signal-Injection Sensorless Control of IPMSMs

Hirotaka Kato[1], Jun-ichi Itoh[1]*, Gyu-Cheol Lim[2], Jung-Ik Ha[2]
1 Department of Science of Technology Innovation, Nagaoka University of Technology, Niigata, Japan
2 Department of Electrical and Computer Engineering, Seoul National University, Seoul, Republic of Korea
*itoh@vos.nagaokaut.ac.jp

***Abstract*—This paper proposes a spatial harmonic compensation method to suppress torque ripple in signal-injection sensorless control of interior permanent magnet synchronous motors (IPMSMs). The proposed method focuses on the estimation error between the actual and estimated rotor positions caused by spatial harmonics and compensates for the sixth-order component by estimating this error. The compensation is based solely on an inductance model and does not require parameter tuning or trial-and-error adjustment. Experimental results demonstrate that the proposed method reduces the sixth-order component of the position estimation error by up to 98.8% and that of the torque ripple by up to 95.3%.**

Keywords— Spatial harmonic compensation, sixth-order ripple, signal-injection sensorless control, torque ripple suppression.

I. Introduction

Recent home appliances require both high efficiency and low cost. For this reason, interior permanent magnet synchronous motors (IPMSMs) have been widely adopted because they are compact, lightweight, and highly efficient [1][2]. To reduce manufacturing costs, motors with concentrated windings are often used and operated without position sensors. However, concentrated-winding IPMSMs tend to exhibit spatial harmonics in the armature inductance, resulting in increased torque ripple [3][4]. This torque ripple can cause mechanical vibration, particularly in the low-speed region.

Signal-injection sensorless control (SISC) is widely studied for position sensorless control in the low-speed region [5–8]. In SISC, a high-frequency signal is injected into the estimated d-axis. Then, only the harmonic component is extracted from the estimated q-axis current. The position estimator is controlled such that the amplitude of this harmonic component becomes zero, which determines the rotor position at which the inductance is minimum. This position corresponds to the motor's d-axis. However, when cross-coupling exists between the d- and q-axes in the inductance, the rotor position at which the inductance is minimum does not coincide with the motor d-axis. Consequently, an estimation error in the rotor position occurs. In particular, in the magnetic saturation region, the influence of dq-axis cross-coupling becomes significant. It has been reported that an offset error remains in the estimated rotor position [5][6]. Furthermore, when SISC is applied to concentrated-winding IPMSMs, the inductance is affected by not only magnetic saturation but also spatial harmonics. Due to this effect, the inductance varies with a period six times that of the electrical angle. This implies that both an offset error and a sixth-order error exist in the estimated rotor position. This phenomenon has been reported in [7] and [8]. These estimation errors degrade the current control performance and consequently increase torque ripple.

A compensation method has been proposed for the offset error in the estimated rotor position caused by dq-axis cross-coupling [9]. This method corrects the current command values while considering pre-calculated position offset errors. This method calculates the offset angle in advance using an inductance model that considers magnetic saturation. Then, the estimated dq-axis current commands are corrected so that the actual dq-axis currents match the desired values. Although the offset error in the estimated rotor position remains, this approach allows the average dq-axis currents to be controlled to the desired values. However, this method does not account for the influence of spatial harmonics. Therefore, it cannot compensate for the ripple error in the estimated position.

On the other hand, ref. [10] has proposed a compensation method for the position estimation error caused by spatial harmonics in the inductance. This method corrects the injection angle of the signal and the amplitude of the detected harmonic current. This method primarily aims to expand the operating range in the zero-saliency region but also considers the influence of spatial harmonics. Specifically, correction values are analyzed in advance for each small change in the rotor position so that the convergence angle of the position estimation observer coincides with the actual rotor position. These correction values are stored in a table and applied during control. However, analyzing the correction values requires trial-and-error adjustments, and the procedure is complex. Furthermore, it has been reported that, even when compensating for the influence of spatial harmonics, a sixth-order error component remains in the estimated rotor position.

This paper proposes a compensation method for rotor position estimation errors caused by spatial harmonics of the inductance in order to suppress torque ripple in SISC of IPMSMs. The proposed method focuses on the fact that the position estimation observer converges to the rotor position at which the inductance is minimum. The convergence angle is defined as the saliency shift angle, which is calculated online using the inductance model. The estimated rotor position is then corrected using the calculated saliency shift angle to obtain a more accurate value. Then, a current command is generated based on the corrected rotor position. Torque ripple is suppressed by adding a sixth-order current component to the current command, thereby canceling the torque ripple. Although the proposed method requires the inductance profile obtained in advance, only the sixth- and twelfth-order components are used in the modeling. Therefore, the computational cost during estimation can be significantly reduced. Additionally, since the saliency shift angle is calculated using a mathematical formula, it does not require trial-and-error analysis. Consequently, the proposed method can easily compensate for the influence of spatial harmonics and effectively suppress torque ripple.

II. Signal-Injection Sensorless Control

Fig. 1 shows the relationship between the rotor reference frame (RRF) and the estimated rotor reference frame (ERRF). In this paper, the error $\tilde{\theta}_r$ is defined as the difference between the actual rotor position θ_r and the estimated rotor position $\hat{\theta}_r$. The symbol $\mathbf{L}^{\mathrm{r}}_{\mathrm{dq}}$ in Fig. 1 represents the inductance ellipse proposed in [10], which illustrates, on the reference frame, the saliency ratio of the inductance and the relationship between the rotor position and the angular position of the saliency as an amplitude. The harmonic model of the IPMSM in the RRF is given by

$$\mathbf{v}^{\mathrm{r}}_{\mathrm{dqh}} = \mathbf{L}^{\mathrm{r}}_{\mathrm{dq}} \frac{\mathrm{d}}{\mathrm{d}t} \mathbf{i}^{\mathrm{r}}_{\mathrm{dqh}}$$
$$\begin{bmatrix} v^r_{dh} \\ v^r_{qh} \end{bmatrix} = \begin{bmatrix} L^r_{dd} & L^r_{dq} \\ L^r_{qd} & L^r_{qq} \end{bmatrix} \frac{\mathrm{d}}{\mathrm{d}t} \begin{bmatrix} i^r_{dh} \\ i^r_{qh} \end{bmatrix} \quad \text{(1)},$$

where L^r_{dq} and L^r_{qd} are cross-coupling inductances. When a position estimation error $\tilde{\theta}_r$ exists between the RRF and the ERRF, eq. (1) can be transformed into the ERRF as follows,

$$\mathbf{R}(\tilde{\theta}_r)\mathbf{v}^{\mathrm{r}}_{\mathrm{dqh}} = \mathbf{R}(\tilde{\theta}_r)\left(\mathbf{L}^{\mathrm{r}}_{\mathrm{dq}} \frac{\mathrm{d}}{\mathrm{d}t} \mathbf{i}^{\mathrm{r}}_{\mathrm{dqh}}\right)$$
$$\mathbf{v}^{\hat{\mathrm{r}}}_{\mathrm{dqsh}} = \mathbf{L}^{\hat{\mathrm{r}}}_{\mathrm{dq}} \frac{\mathrm{d}}{\mathrm{d}t} \mathbf{i}^{\hat{\mathrm{r}}}_{\mathrm{dqsh}} \quad \text{(2)},$$
$$\begin{bmatrix} v^{\hat{r}}_{dh} \\ v^{\hat{r}}_{qh} \end{bmatrix} = \begin{bmatrix} L^{\hat{r}}_{dd} & L^{\hat{r}}_{dq} \\ L^{\hat{r}}_{qd} & L^{\hat{r}}_{qq} \end{bmatrix} \frac{\mathrm{d}}{\mathrm{d}t} \begin{bmatrix} i^{\hat{r}}_{dh} \\ i^{\hat{r}}_{qh} \end{bmatrix}$$

where

$$\begin{cases} \mathbf{R}(\tilde{\theta}_r) = \begin{bmatrix} \cos\tilde{\theta}_r & \sin\tilde{\theta}_r \\ -\sin\tilde{\theta}_r & \cos\tilde{\theta}_r \end{bmatrix} \\ L^{\hat{r}}_{dd} = \Sigma L_h - \sqrt{\Delta L^2 + L^2_{dq}} \cos\left(2\tilde{\theta}_r - 2\phi_\Delta\right) \\ L^{\hat{r}}_{dq} = L^{\hat{r}}_{qd} = -\sqrt{\Delta L^2 + L^2_{dq}} \sin\left(2\tilde{\theta}_r - 2\phi_\Delta\right) \\ L^{\hat{r}}_{qq} = \Sigma L + \sqrt{\Delta L^2 + L^2_{dq}} \cos\left(2\tilde{\theta}_r - 2\phi_\Delta\right) \\ \Sigma L = \dfrac{L^r_d - L^r_q}{2} \\ \Delta L = \dfrac{L^r_d - L^r_q}{2} \\ \phi_\Delta = \dfrac{1}{2}\arctan\left(-\dfrac{L^r_{dq}}{\Delta L}\right) \end{cases} \quad \text{(3)}.$$

Here, superscript "r̂" stands for the ERRF. ϕ_Δ is the saliency shift angle. The saliency shift angle represents the angular deviation between the d-axis of the RRF and the orientation of the inductance ellipse shown in Fig. 1. In this paper, the square-wave signal-injection method proposed in [11] is applied. The signal injected into the ERRF is expressed by,

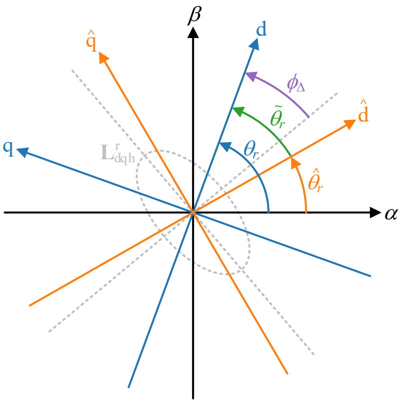

Fig. 1. Relationship between RRF and ERRF.

$$\mathbf{v}^{\hat{\mathrm{r}}}_{\mathrm{dqh}}[n] = \begin{bmatrix} V_h \cdot clk[n] \\ 0 \end{bmatrix} \quad \text{(4)},$$

Here, V_h is the amplitude of the injected square-wave signal. $clk[n]$ is a clock signal that outputs 1 and -1 at every sampling period T_s. The harmonic current amplitude at the sampling instant n is expressed as follows using (2) and (3),

$$\begin{aligned} \Delta\mathbf{i}^{\hat{\mathrm{r}}}_{\mathrm{dqh}}[n] &= \mathbf{i}^{\hat{\mathrm{r}}}_{\mathrm{dqh}}[n] - \mathbf{i}^{\hat{\mathrm{r}}}_{\mathrm{dqh}}[n-1] \\ &= \begin{bmatrix} I_\Sigma + I_\Delta \cos\left(2\tilde{\theta}_r - 2\phi_\Delta\right) \\ I_\Delta \sin\left(2\tilde{\theta}_r - 2\phi_\Delta\right) \end{bmatrix} \cdot clk[n-2] \quad \text{(5)}, \\ &= \begin{bmatrix} \Delta i^{\hat{r}}_{dh}[n] \\ \Delta i^{\hat{r}}_{qh}[n] \end{bmatrix} \end{aligned}$$

where

$$\begin{cases} I_\Delta = \dfrac{V_h T_s \Sigma L}{L_{dd}L_{qq} - L^2_{dq}} \\ I_\Sigma = \dfrac{V_h T_s \sqrt{L^2_{dq} + \Delta L^2}}{L_{dd}L_{qq} - L^2_{dq}} \end{cases} \quad \text{(6)}.$$

The calculated value of the position estimation error $\tilde{\theta}_{r,calc}[n]$ can be obtained using $\Delta i^{\hat{r}}_{qh}[n]$ as follows,

$$\tilde{\theta}_{r,calc}[n] = \frac{\Delta i^{\hat{r}}_{qh}}{2I_\Delta} \cdot clk[n-2] = \frac{1}{2}\sin\left(2\tilde{\theta}_r - 2\phi_\Delta\right) \quad \text{(7)}.$$

In SISC, the position estimation observer is controlled so that $\tilde{\theta}_{r,calc}$ becomes zero. Under this condition, the following relationship holds,

$$\hat{\theta}_r = \theta_r - \tilde{\theta}_r \approx \theta_r - \phi_\Delta \quad \text{(8)}.$$

Eq. (8) indicates that the estimated rotor position is offset from the actual rotor position by ϕ_Δ.

Table 1 shows the specifications of the test motor, Fig. 2 shows its inductance characteristics, and Fig. 3 shows the ϕ_Δ characteristics. Fig. 3 is obtained from the inductance data in Fig. 2 using (3). The test motor has a 6-pole, 9-slot salient-pole concentrated-winding structure. As shown in Fig. 2, the inductance exhibits a sixth-order error that varies with the rotor position. In addition, comparison between Fig. 2(a) and (b) shows that magnetic saturation also causes inductance variation. From Fig. 3, it can be seen that the position estimation error includes a sixth-order component caused by the spatial harmonics of the inductance, and that in the high-torque region, an offset component due to magnetic saturation is superimposed.

III. Proposed Spatial Harmonic Compensation Method

A. Principle of Proposed Compensation Method

Fig. 4 shows an overview of the proposed method. From (8), it is evident that the estimation error corresponds to the saliency shift angle ϕ_Δ. Therefore, by estimating ϕ_Δ, it is possible to correct the error in $\hat{\theta}_r$, denoted as $\tilde{\theta}_r$. In the proposed method, ϕ_Δ is estimated separately in addition to $\hat{\theta}_r$, and $\hat{\theta}_r$ is corrected using $\hat{\phi}_\Delta$ to obtain more accurate position information. Since ϕ_Δ is estimated without a speed-dependent resonance filter, the method remains stable even at zero speed. The computation relies solely on the inductance model and does not require parameter tuning or trial-and-error adjustment.

To account for the effects of spatial harmonics, this paper employs an inductance model for control that is formulated using a constant term and pulsating components for each harmonic order. When the motor only operates on the MTPA trajectory, the motor inductance can be expressed as a function of the torque T_e and rotor position θ_r as follows,

$$\mathbf{L}^r_{dq}(T_e,\theta_r)=\begin{bmatrix} L^r_{dd}(T_e,\theta_r) & L^r_{dq}(T_e,\theta_r) \\ L^r_{qd}(T_e,\theta_r) & L^r_{qq}(T_e,\theta_r)\end{bmatrix} \quad \text{(9)},$$

where

$$L^r_{ij}(T_e,\theta_r)=L^r_{ij-0}(T_e) + \sum_{k=1}^{n} L^r_{ij-6ka}(T_e)\cdot\cos 6k\theta_r + \sum_{k=1}^{n} L^r_{ij-6kb}(T_e)\cdot\sin 6k\theta_r \quad , i,j\in\{d,q\} \quad \text{(10)}.$$

When the estimation error between the compensated estimated rotor position $\hat{\theta}_{r,cmp}$ and the actual rotor position θ_r is sufficiently small, the following relationship holds,

$$L^r_{ij}(T_e,\theta_r)\approx L^r_{ij}(T_e^*,\hat{\theta}_{r,cmp}) \quad , i,j\in\{d,q\} \quad \text{(11)}.$$

Here, T_e^* is the torque command within the controller. Following the same procedure as in (3), the estimated saliency shift angle $\hat{\phi}_\Delta$ is obtained as follows,

$$\hat{\phi}_\Delta=\frac{1}{2}\arctan\left(-\frac{L^r_{dq}}{\Delta L}\right) \quad \text{(12)},$$

where

$$\begin{cases} \Delta\hat{L}=\dfrac{\hat{L}^r_d-\hat{L}^r_q}{2} \\ \hat{\phi}_\Delta=\dfrac{1}{2}\arctan\left(-\dfrac{\hat{L}^r_{dq}}{\Delta\hat{L}}\right)\end{cases} \quad \text{(13)}.$$

Table 1. Specifications of test motor.

Parameter	Value
Rated Power	1.5 kW
Base Speed	3600 r/min
Rated Torque	4.0 Nm
Rated Current	4.4 A_{rms}
DC Link Voltage	300 V
Pole / Slot	6 / 9
Overall Inertia	170×10^{-4} kg·m^2
Winding Resistance	307 mΩ
dq-axis Inductance (no-load)	L_d=5.4 mH, L_q=9.5 mH

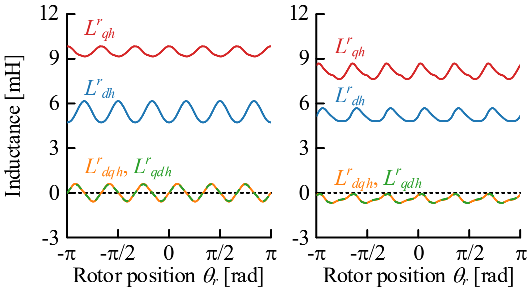

Fig. 2. Inductance characteristics.

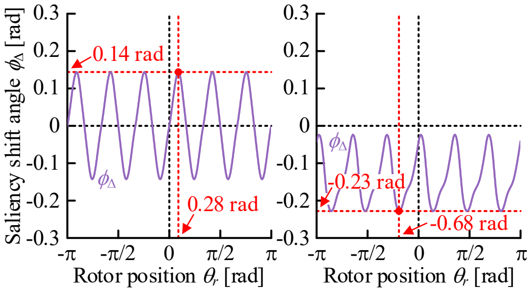

Fig. 3. ϕ_Δ characteristics.

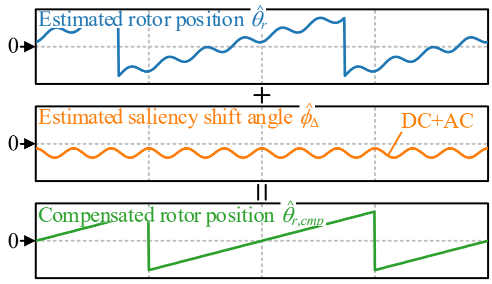

Fig. 4. Relationship between RRF and ERRF.

Eq. (6) and (7) are derived under the assumption that $\hat{\theta}_{r,cmp}\approx\theta_r$, and under this condition, $\hat{\phi}_\Delta\approx\phi_\Delta$ holds. In the proposed method, $\hat{\phi}_\Delta$ is calculated using $\hat{\theta}_{r,cmp}$, and the phase error is compensated as $\hat{\theta}_{r,cmp}=\hat{\theta}_r+\hat{\phi}_\Delta$. To prevent recursive computation in the calculation process of $\hat{\phi}_\Delta$, a low-pass filter (LPF) is placed after the ϕ_Δ estimator. The inductance identification of the actual machine is performed using the method described in [12].

Fig. 5 shows the block diagram of the proposed control system. In the proposed method, different estimated rotor positions are used for the position estimator and the current controller; thus, the two reference frames are implemented

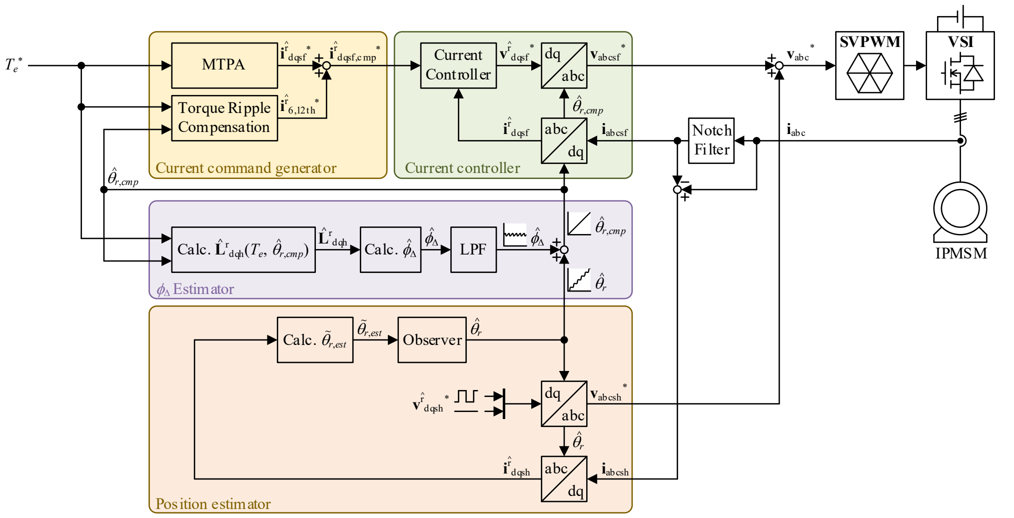

Fig. 5. Block diagram of proposed method.

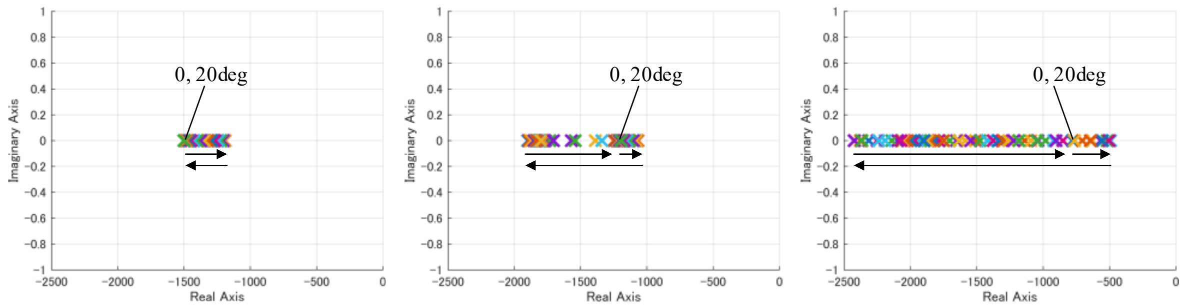

(a) $T_e = 0$ (b) $T_e = 4$ Nm (1p.u.) (c) $T_e = 6$ Nm (1.5p.u.)

Fig. 6. Stability analysis results of ϕ_Δ estimator.

separately. In addition, based on the accurate rotor position information, a current command capable of suppressing torque ripple as proposed in [13] is applied.

B. Stability Analysis

In this section, the stability of the proposed ϕ_Δ estimator is analyzed. Assuming that the dq-axis currents are not affected by the rotor position error, the response from the estimated rotor position $\hat{\theta}_r$ to the compensated estimated rotor position $\hat{\theta}_{r,cmp}$ can be expressed as follows,

$$\begin{cases} p\hat{\phi}_\Delta = -\omega_c\hat{\phi}_\Delta \\ \qquad + \dfrac{\omega_c}{2}\arctan\left[\dfrac{2L_{dqh}(T_e^*,\hat{\theta}_r+\hat{\phi}_\Delta)}{L_{qh}(T_e^*,\hat{\theta}_r+\hat{\phi}_\Delta)-L_{dh}(T_e^*,\hat{\theta}_r+\hat{\phi}_\Delta)}\right] \\ \hat{\theta}_{r,cmp} = \hat{\phi}_\Delta + \hat{\theta}_r \end{cases} \quad \text{...(14)},$$

where ω_c is the cutoff frequency of the LPF. By linearizing (14) around the steady-state operating point, the following equation is obtained,

$$\begin{cases} p\Delta\hat{\phi}_\Delta = \mathbf{A}\Delta\hat{\phi}_\Delta + \mathbf{B}\Delta\hat{\theta}_r \\ \Delta\hat{\theta}_{r,cmp} = \mathbf{C}\Delta\hat{\theta}_r + \mathbf{D}\Delta\hat{\phi}_\Delta \end{cases} \quad \text{......................................(15)},$$

where

$$\begin{cases} \mathbf{A} = \omega_c\left[-1+\dfrac{\dfrac{\partial L_{dqh}}{\partial\theta_r}\left(L_{qh0}-L_{dh0}\right)-\left(\dfrac{\partial L_{qh}}{\partial\theta_r}-\dfrac{\partial L_{dh}}{\partial\theta_r}\right)L_{dqh0}}{\left(L_{qh0}-L_{dh0}\right)^2+4L_{dqh0}^2}\right] \\ \mathbf{B} = \omega_c\dfrac{\dfrac{\partial L_{dqh}}{\partial\theta_r}\left(L_{qh0}-L_{dh0}\right)-\left(\dfrac{\partial L_{qh}}{\partial\theta_r}-\dfrac{\partial L_{dh}}{\partial\theta_r}\right)L_{dqh0}}{\left(L_{qh0}-L_{dh0}\right)^2+4L_{dqh0}^2} \\ \mathbf{C} = 1 \\ \mathbf{D} = -1 \end{cases} \quad .\ (16).$$

Subscript "0" stands for the steady-state value.

Fig. 6 shows the results of the pole placement analysis. In Fig.6, the stability is evaluated by pole placement using (16). In the analysis, ω_c=1500 rad/s was used, and the evaluation was conducted while varying the torque from 0 to 1.5p.u. Since the motor inductance exhibits periodic symmetry, the rotor position is analyzed in the range of 0-20 degrees. From Fig. 6, it can be observed that the poles always remain on the negative real axis even when the rotor position changes, confirming that the proposed ϕ_Δ estimator is stable at all operating points.

IV. Experimental Results

Fig. 9 shows the experimental system. An induction machine is used on the load side of the test system, and the torque control performance of the test motor is evaluated by controlling the speed of the induction machine. To validate the proposed method, the behavior of the proposed estimator is first verified through simulation. Then, the position estimation performance and torque ripple are evaluated using experimental results.

Fig. 10 shows the behavior of the position estimator and the ϕ_Δ estimator in simulation. In both the simulation and experimental verification, the switching frequency is set to 5 kHz, the current control bandwidth to 1500 rad/s, the position observer bandwidth to 150 rad/s, and the cutoff frequency of the LPF for recursive computation suppression to 1500 rad/s. As shown in Fig. 10, although $\tilde{\theta}_{r,est}$ is regulated to zero by the position observer, the conventional method results in a sixth-order error with an additional offset superimposed on $\tilde{\theta}_r$. In contrast, in the proposed method, these components are suppressed by correcting $\hat{\theta}_r$ to $\hat{\theta}_{r,cmp}$ using $\hat{\phi}_\Delta$. Furthermore, $\hat{\phi}_\Delta$ accurately estimates ϕ_Δ, confirming the effectiveness of the ϕ_Δ estimator. The residual ripple in $\tilde{\theta}_r$ is of the 18th order, which arises because the inductance was modeled using the sixth- and twelfth-order components. Thus, the proposed method selectively compensates for specified harmonic components in the rotor position estimation error.

Fig. 11 shows the experimental results at a speed of 0.01p.u. and a torque of 0.5p.u. As in Fig. 11, the proposed method effectively compensated for the sixth-order component of the position estimation error. In addition, the output torque was kept constant by the current command designed to suppress torque ripple.

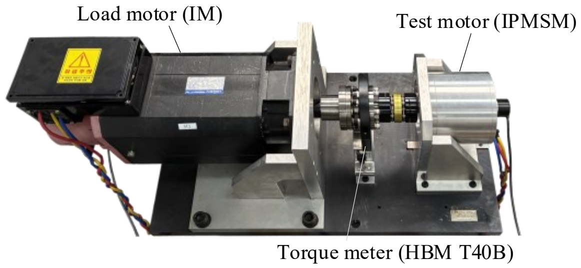

Fig. 9. Experimental system.

Fig. 12 shows the experimental results when a step torque command at rated torque is applied at zero speed. The proposed method successfully followed the command without losing synchronism, similar to the conventional method.

Fig. 13 shows the analysis results of the sixth-order component of the position estimation error and torque ripple. With the proposed method, the sixth-order component of the position estimation error was reduced by up to 98.8%, and that of the torque ripple by up to 95.3%. Although the reduction effect slightly decreases under high-torque operation, this was considered to result from the limited response of the position observer. Even at very low speeds, it is difficult to completely eliminate the ripple component appearing in θ_r, and in simulations, the reduction ratios of the sixth-order position estimation error were 80.6% and 81.3% at operating points of 0 and 1p.u. torque at a speed of 0.01p.u., respectively. The reduction in compensation performance caused by the observer's response limitation will be addressed in future work.

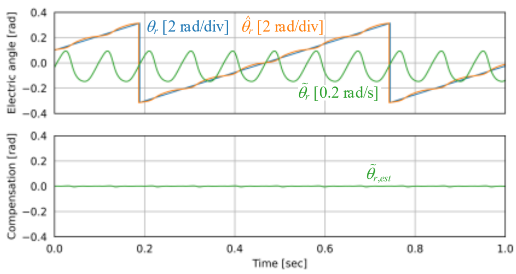

(a) Conventional method.

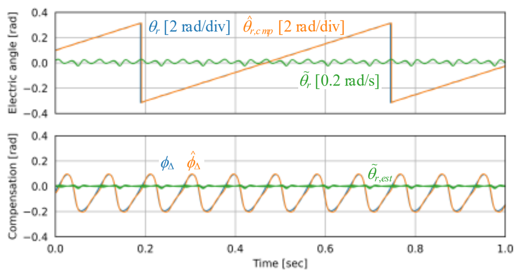

(b) Proposed method.

Fig. 10. Simulation: Position tracking performance and behavior of ϕ_Δ estimator (ω_m = 0.01p.u., T_e = 0.5p.u.).

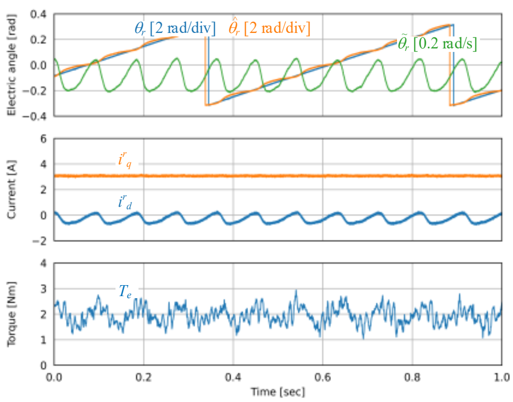

(a) Conventional method.

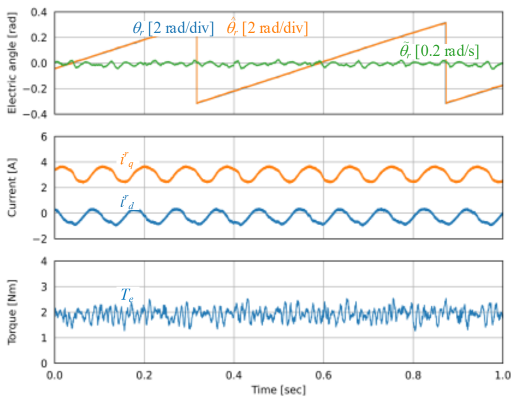

(b) Proposed method.

Fig. 11. Experiment 1: Steady-states operation (ω_m = 0.01p.u., T_e = 0.5p.u.).

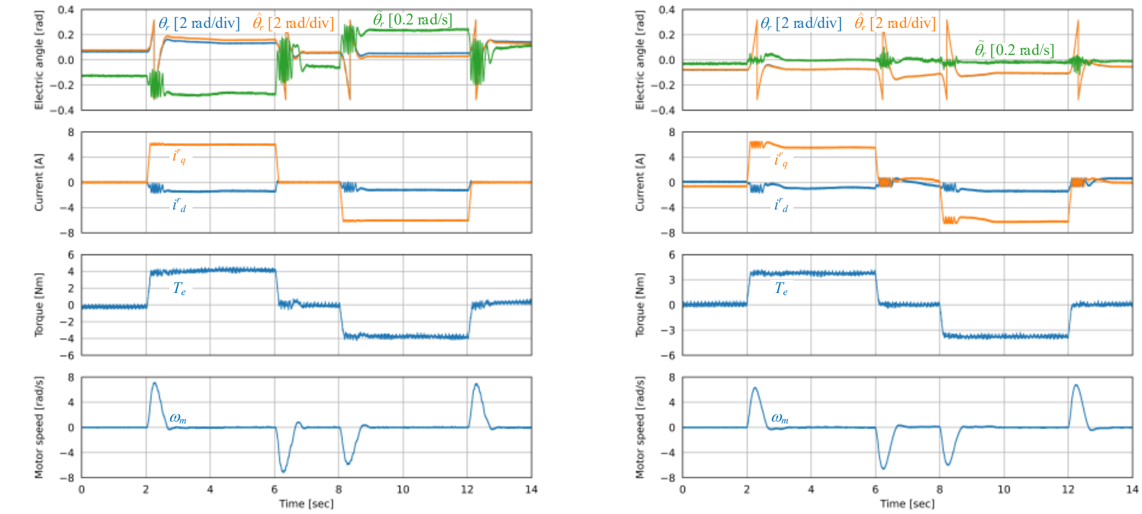

(a) Conventional method. (b) Proposed method.

Fig. 12. Experiment 2: Step torque response at standstill (ω_m = 0, T_e = 0 to 1p.u.).

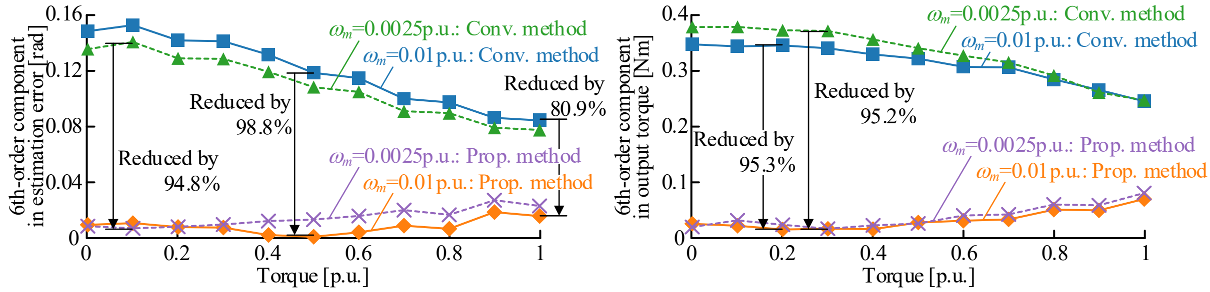

(a) Estimation error. (b) Output torque.

Fig. 13. Comparison results of sixth-order component in experiment.

V. Conclusion

This paper has proposed a model-based spatial harmonic compensation method for torque ripple reduction in signal-injection sensorless control of IPMSMs. The proposed method compensates for the sixth-order position estimation error caused by spatial harmonics. The compensation is achieved by estimating the phase to which the position observer converges, i.e., the minimum inductance phase. Experimental results demonstrated that the proposed method reduced the sixth-order component of the position estimation error by up to 98.8% and that of the torque ripple by up to 95.3%, thereby confirming its effectiveness.

Acknowledgment

This work was supported by JST SPRING, Japan Grant Number JPMJSP2189.

References

[1] S. Morimoto, Y. Shimizu, Y. Inoue and M. Sanada, “Experimental Evaluation of the Online MTPA Angle Search Method Based on Flux-linkage Plane Estimation for IPMSMs,” in IEEJ Journal of Industry Applisations, vol. 13, no. 4, pp. 400-408, 2024

[2] Y. Inoue, S. Morimoto and M. Sanada, “Mathematical Model of MTPA Control for M- and T-axis Current Control Systems in PMSM Drives,” in IEEJ Journal of Industry Applisations, vol. 14, no. 3, pp. 395-401, 2025

[3] G. -H. Lee, S. -I. Kim, J. -P. Hong and J. -H. Bahn, “Torque Ripple Reduction of Interior Permanent Magnet Synchronous Motor Using Harmonic Injected Current,” in IEEE Transactions on Magnetics, vol. 44, no. 6, pp. 1582-1585, June 2008

[4] S. Yamamoto and Y. Hidaka, “Torque Ripple Reduction in Specific Directions for Concentrated Winding IPM Motors Using Cogging Torque Phase Shift by Asymmetric Flux Barriers,” in IEEE Transactions on Industry Applications, vol. 62, no. 2, pp. 2598-2610, March-April 2026

[5] P. Guglielmi, M. Pastorelli and A. Vagati, “Cross-Saturation Effects in IPM Motors and Related Impact on Sensorless Control,” in IEEE Transactions on Industry Applications, vol. 42, no. 6, pp. 1516-1522, Nov.-dec. 2006

[6] D. Diaz Reigosa, P. Garcia, D. Raca, F. Briz and R. D. Lorenz, "Measurement and Adaptive Decoupling of Cross-Saturation Effects and Secondary Saliencies in Sensorless Controlled IPM Synchronous Machines," in *IEEE Transactions on Industry Applications*, vol. 44, no. 6, pp. 1758-1767, Nov.-dec. 2008

[7] M. W. Degner and R. D. Lorenz, “Using multiple saliencies for the estimation of flux, position, and velocity in AC machines,” in IEEE Transactions on Industry Applications, vol. 34, no. 5, pp. 1097-1104, Sept.-Oct. 1998

[8] Zhong, Z., Shao, Z. & Zhou, S. “Initial rotor position estimation by pulsating high-frequency voltage injection considering mutual inductance,” J. Power Electron. 21, 1484–1492 2021

[9] Jin, N., Li, G., Zhou, K. et al, “MTPA Trajectory Tracking Control with On-line MRAS Parameter Identification for an IPMSM,” J. Electr. Eng. Technol. 14, 2355–2366 2019

[10] Y. -C. Kwon, J. Lee and S. -K. Sul, “Extending Operational Limit of IPMSM in Signal-Injection Sensorless Control by Manipulation of Convergence Point,” in IEEE Transactions on Industry Applications, vol. 55, no. 2, pp. 1574-1586, March-April 2019

[11] Y. -D. Yoon, S. -K. Sul, S. Morimoto and K. Ide, “High-Bandwidth Sensorless Algorithm for AC Machines Based on Square-Wave-Type Voltage Injection,” in IEEE Transactions on Industry Applications, vol. 47, no. 3, pp. 1361-1370, May-June 2011

[12] H. -S. Kim and S. -K. Sul, “Real-Time Torque Control of IPMSM Under Flux Variations,” in IEEE Journal of Emerging and Selected Topics in Power Electronics, vol. 10, no. 3, pp. 3345-3356, June 2022

[13] T. Nishio, R. Yamauchi, M. Kondo and K. Akatsu, “An Injected High Frequency Current Reference Generation Method for Torque Ripple Reduction in PMSM,” in IEEJ Transactions on Industry Applications, vol. 141, no. 11, pp. 848-855, 2021